Original paper

Position of Ti^{4+} in the tourmaline structure based on bond-valence topological modelling

Peter BAČÍK[1,*], Lenka SKŘÁPKOVÁ[1,2]

[1] *Comenius University in Bratislava, Faculty of Natural Sciences, Department of Mineralogy, Petrology and Economic Geology, Ilkovičova 6, 842 15 Bratislava, Slovak Republic; peter.bacik@uniba.sk*
[2] *Masaryk University, Department of Geological Sciences, Kotlářská 2, 61137 Brno, Czech Republic*
[*] *Corresponding author*

Tourmalines commonly contain minor amounts of Ti. However, Ti-rich compositions are relatively rare, with only two approved tourmaline species – dutrowite and magnesio-dutrowite, showing significant Ti^{4+} occupancy at the *Y* site. According to the currently valid tourmaline nomenclature, Ti^{4+} is assigned exclusively to the *Y* site. To evaluate the structural mechanisms capable of introducing Ti^{4+} into the tourmaline structure, a series of modelled mechanisms was examined to identify the most plausible and locally stable arrangements involving Ti. For this purpose, short-range bond-valence requirements, distortion indices characterizing local polyhedral geometry, and long-range constraints expressed through the <*Y*–O> and <*Z*–O> ratios were applied to assess the likelihood of individual components containing Ti^{4+} at various crystallographic sites and within different local environments. Most tested structural mechanisms exhibited severe anion underbonding, overbonding, or produced unrealistic distortion indices. Nevertheless, the calculations indicate that Ti^{4+} can, in principle, be accommodated at the *Y*, *Z*, and even *T* sites, and prove that its higher valence and larger cation size are efficiently redistributed within the structure. The total amount of Ti^{4+} appears to be structurally limited to approximately one *apfu*, as higher Ti^{4+} contents (> 1 *apfu*) lead to substantial structural deformation resulting in an unstable arrangement.

Keywords: tourmaline supergroup; titanium; crystal chemistry; bond valence topological model; bond valence topological field; crystal-chemical stability
Received: December 16, 2025; accepted: June 16, 2026; handling editor: F. Bosi
The online version of this article (doi: 10.3190/jgeosci.0052.25) contains supplementary electronic material.

1. Introduction

Tourmaline-supergroup minerals are silicates crystallizing in the space group *R*3*m* and have the general formula $XY_3Z_6(T_6O_{18})(BO_3)_3V_3W$ (Hawthorne and Henry 1999). The most common ions at each site are: *X* = Na^+, Ca^{2+}, K^+, and site vacancy; *Y* = Fe^{2+}, Mg^{2+}, Mn^{2+}, Al^{3+}, Li^+, Fe^{3+}, Cr^{3+}, and V^{3+}; *Z* = Al^{3+}, Fe^{3+}, Mg^{2+}, Cr^{3+}, and V^{3+}; *T* = Si^{4+}, Al^{3+}, and B^{3+}; *B* = B^{3+}; *V* = OH^- and O^{2-}; and *W* = OH^-, F^-, and O^{2-} (Henry et al. 2011). The structure (Fig. 1) contains 5 different cation crystallographic sites with various coordination – tetrahedral *T* site, two different octahedral *Z* and *Y* sites, polyhedral 9-coordinated *X* site, triangular *B* site, and eight different anion sites – O1–O8 (Donnay and Buerger 1950). Titanium can occur at the *Y* and *Z* sites, and possibly also at the *T* site. However, owing to the significantly longer bonds compared to Si^{4+}, its presence at the *T* site is unlikely, although not impossible (Bačík and Fridrichová 2021).

Tourmalines containing significant amounts of Ti, are quite uncommon, and currently there are only two approved tourmaline species with Ti^{4+} at the *Y* site, dutrowite (Biagioni et al. 2023) and magnesio-dutrowite (Pieczka et al. 2023). However, many studies described tourmaline species with minor but significant amounts of Ti^{4+} at the *Y* site, typically uvite-feruvite series with up to 0.35 *apfu* Ti^{4+} (e.g., Jiang et al. 1996; Grice and Robinson 1989; Selway et al. 1998; Scribner et al. 2018; Gadas et al. 2014, 2023), schorl-dravite series up to 0.32 *apfu* Ti^{4+} (e.g., Henry and Dutrow 1996; Pesquera and Velasco 1997; Povondra et al. 1998; Bloodaxe et al. 1999; Cámara et al. 2002; Bosi and Lucchesi 2004; Bosi et al. 2005, 2012; Pesquera et al. 2005; Bačík et al. 2008, 2013, 2022; Bosi 2008; Baksheev et al. 2010; Clark et al. 2011; Ertl et al. 2010, 2012; Scribner et al. 2018; Harlaux et al. 2020) or povondraite with up to 0.56 *apfu* (Žáček et al. 2000; Bačík et al. 2008; Bosi et al. 2013, 2023; Watenphul et al. 2016). Žáček et al. (2000) characterised tourmaline of povondraite composition with 0.56 apfu Ti; unfortunately, the crystal structure was not determined. Vereshchagin et al. (2022) experimentally synthesized dravite with 0.27 *apfu* Ti^{4+} and described the positive correlation between the low pressure and the incorporated amount of Ti. Jiang et al. (1996) described feruvites with Ti^{4+} assigned also to the *Z* and *T* sites, which is very unusual; however, based on the site allocation rules in Henry et al. (2011), all Ti^{4+} should be assigned to the *Y* site, and for the purposes of this study, all chemical analyses of Jiang et al. (1996) were recalculated.

Published under Creative Commons Attribution-NonCommercial 4.0 International (CC BY-NC 4.0) license

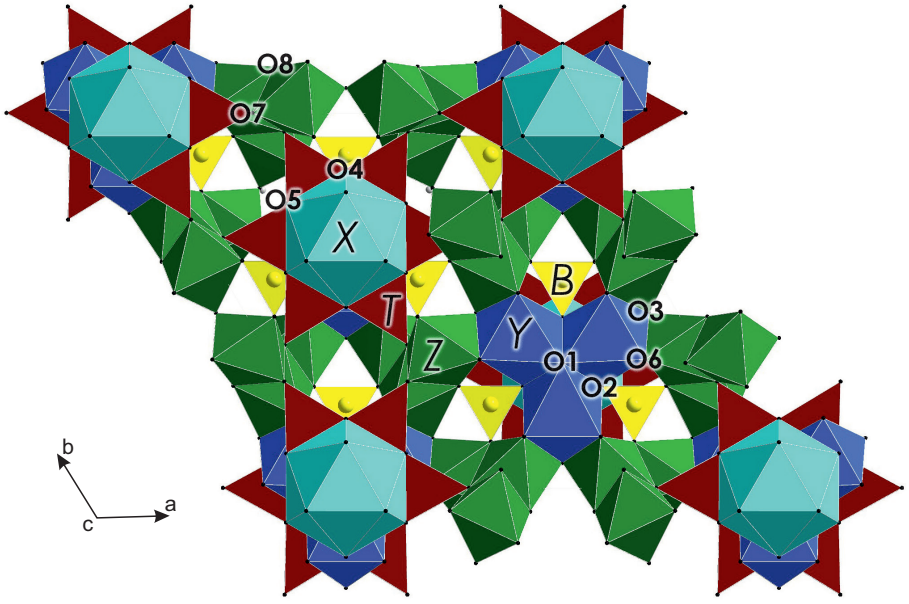
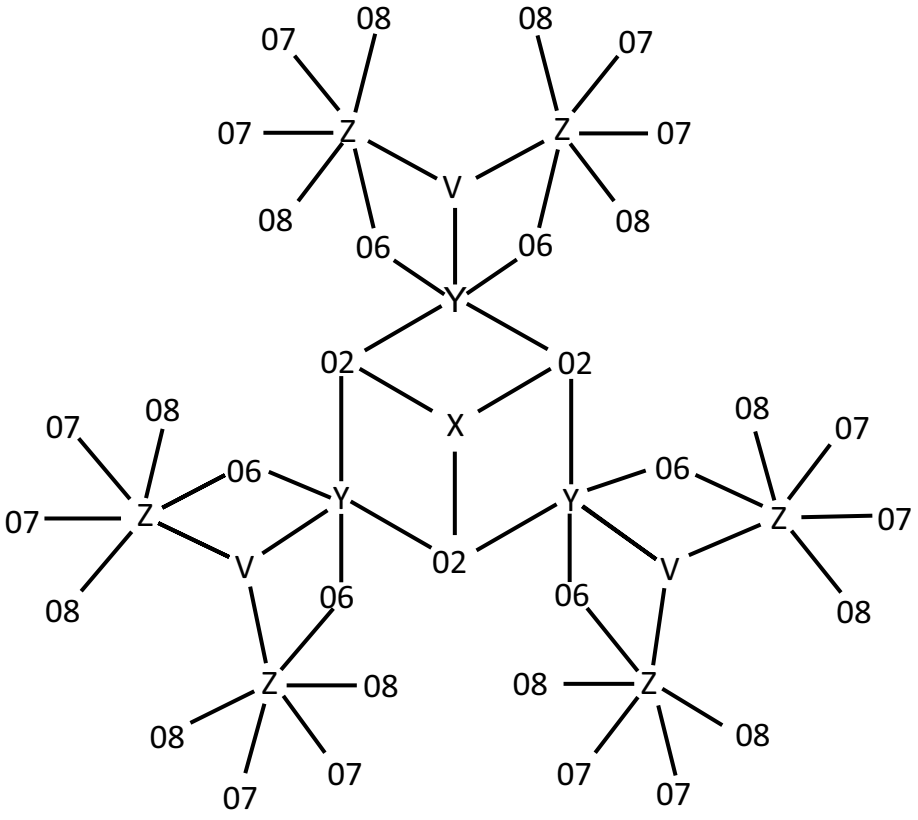


Fig. 1 The structure of tourmaline-supergroup minerals with highlighted structural sites. Based on the structure of dutrowite (Biagioni et al. 2023).

Titanium in tourmaline is almost always considered to be four-valent, although some spectroscopic interpretations assume intervalence charge transfer transitions (IVCT) between Ti^{3+}–Ti^{4+} and Ti^{3+}–Ti^{4+}–Fe^{3+} (da Fonseca-Zang et al. 2008). However, this is not supported by the structural data. Even though the presence of Ti^{3+} was determined in meteorites or mantle-derived silicates (Ma and Rossman 2009; Oliveira et al. 2021; Ma et al. 2023), for the purpose of this paper, titanium is solely considered to be Ti^{4+}. In crustal conditions, Ti^{3+} is restricted to highly reducing environments (Borisov 2012; Kommescher et al. 2023), which are extremely rare during tourmaline crystallization.

The goal of this paper is to identify the structural mechanisms that can introduce Ti^{4+} into the tourmaline structure, determine the most likely local arrangements involving Ti, and test their stability. For these purposes, the short-range bond valence constraints, the distortion indices describing the local geometry, and the long-range (<*Y*-O> and <*Z*-O> ratio) constraints were applied to determine the likelihood of proposed components containing Ti^{4+} at various sites and in various local arrangements.



2. Methods

Possible structural arrangements involving Ti^{4+} in tourmaline were studied with the bond-valence topological modelling (BVTM, Bačík 2026), and the bond-valence topological field (BVTF, Bačík 2026).

Fig. 2 The topological graph of three *Y* and neighbouring six *Z* sites.

Bond-length calculations use the following equation:

$$d_{ij} = R_0 - b \ln v_{ij}$$

where d_{ij} is the bond length (in Å) between the two ions, the bond valence (v_{ij}) is their bond strength (in *vu* – valence units), R_0 is the unit bond length, and b is the universal parameter for each bond (Brown 2016). The R_0 and b values for each cation are taken from the list of Gagné and Hawthorne (2015).

Firstly, a bond-valence topological graph (BVTG) with crystallographic sites as nodes and bonds as edges for the studied structural segment was prepared (Fig. 2). Secondly, the bond-valence topological model was applied with respect to the following steps (Bačík 2026).

2.1. Proposing possible components

A *component* is defined by the composition of the structural fragment, which obeys the following rules: 1) the split occupancy at a unique node in the structural arrangement is not allowed; 2) the structural stability is required. The unique node is treated not as every instance of that specific structural site within the arrangement. When the structural site occurs multiple times in the arrangement, each node can be occupied by exactly one atom, molecule, or vacancy.

2.2. Construction of initial models:

2.2.1. Construction of BVTM for each component with ideal values

The model for each component, with bond valence values attached to each edge of the graph (bond), was calculated. For the calculation, the program BoVaToM 1.2 (https://kmplg.sk/?page_id=3275) was used, following these rules for the determination of bond valence values:

1) The Bond-Valence Sum (BVS) rule – the sum of bond valences at each ion should be equal to the formal valence (FV).
2) If the formal charge of an ion at the specific site changes, stronger bonds obtain a larger increase and a smaller decrease in bond valence than weaker bonds to satisfy electrostatic forces in the structure (Brown 2016).
3) The change in FV of any coordinated ion requires a commensurate change in incident bond strengths, such that the valence sum rule is maintained – large differences in bond valences of one site produce large to even unreasonable distortion of the site, which results in unstable local structural arrangements (Bačík 2026).

2.2.2. Construction of BVTF

The construction of BVTF is based on transforming the edges of BVTG into points of BVTF based on their spatial positions (Bačík 2026). This allows the calculations of bond valence and bond length values at each point, resulting in BVTF, which is represented by the colour gradient.

2.3. Testing of initial models

The stability of components can be evaluated by both short-range and long-range structural constraints. Short-range stability can be determined using the Bond Valence Theory (Hawthorne 2002). There are two possible criteria for assessing structural stability: 1) realistic bond lengths and 2) realistic bond-valence arrangements.

2.4. Refinement of models

During refinement, the bond-valence values for each bond-valence topological graph are corrected according to empirical data

The refined values followed these requirements: (1) BVS should not differ from cation and anion FV significantly (difference of <0.2 *vu*); (2) at the same site with the same occupancy at neighbouring sites, the refinement values are the same for all arrangements; (3) different occupancy at neighbouring sites was always considered in calculation.

2.5. Testing of refined models

Component stability is evaluated based on short- and long-range structural constraints. The bond-valence values of disordered dravite, $Na(Mg_2Al)(Al_5Mg)Si_6O_{18}(BO_3)_3(OH)_3OH$, were used as an initial model for the bond-valence calculations reflecting heterovalent substitutions. Dravite was chosen because the holotype samples of dutrowite (Biagioni et al. 2023) and magnesio-dutrowite (Pieczka et al. 2023) contain a significant amount of Mg, which favours dravite; however, the modelling would also work with Fe-dominant tourmaline end members.

2.6. Bond length distortion calculations

Octahedral bond length distortion DI (*M*-O) was calculated as

$$\mathrm{DI}\ \ (M-O) = \left(\sum_{i=1}^{6} |d_i - d_m|\right) / (6 \times d_m),$$

Tab. 1 Proposed Ti-bearing components ordered according to the *X*-, then *V*-, and finally *W*-site occupancy.

	X	*Y*			*Z*			*T*		*V*		*W*
0	Na	Mg	Mg	Al	Al_5	Mg		Si_6		OH_3		OH
1	Na	□	Al	Al	Al_6			Si_5	Ti	OH_3		OH
2	Na	Mg	Mg	Al	Al_5	Mg		Si_5	Ti	OH_3		OH
3	Na	Mg	Mg	Mg	Al_5	Ti		Si_5	Al	OH_3		OH
4	Na	Mg	Al	Ti	Al_4	Mg_2		Si_5	Al	OH_3		OH
5	Na	Mg	Mg	Mg	Al_4	Mg	Ti	Si_6		OH_3		OH
6	Na	Mg	Mg	Al	Al_3	Mg_2	Ti	Si_6		OH_3		OH
7	Na	Mg	Mg	Ti	Al_5	Mg		Si_6		OH_3		O
8	Na	Mg	Al	Ti	Al_4	Mg_2		Si_6		OH_3		O
9	Na	Mg	Mg	Mg	Al_5	Ti		Si_6		OH_3		O
10	Na	Mg	Al	Ti	Al_5	Mg		Si_5	Al	OH_3		O
11	Na	Mg	Al	Ti	Al_6			Si_5	Al	O_2	OH	OH
12	Na	Mg	Mg	Al	Al_5	Ti		Si_6		O_2	OH	OH
13	Na	Al	Al	Al	Al_5	Ti		Si_5	Al	O_3		OH
14	Na	Mg	Al	Ti	Al_6			Si_6		O_3		OH
15	Na	Al	Al	Mg	Al_5	Ti		Si_6		O_3		OH
16	□	Mg	Mg	Ti	Al_5	Mg		Si_6		OH_3		OH
17	□	Mg	Mg	Mg	Al_5	Ti		Si_6		OH_3		OH
18	□	Mg	Al	Ti	Al_5	Mg		Si_6		OH_3		O
19	□	Al	Al	Ti	Al_6			Si_4	Al_2	OH_3		O
20	□	Al	Al	Mg	Al_5	Ti		Si_5	Al	OH_3		O
21	□	Mg	Mg	Mg	Al_4	Ti_2		Si_6		OH_3		O
22	□	Ti	Ti	Mg	Al_6			Si_6		O_3		OH
23	Ca	Mg	Mg	Ti	Al_5	Mg		Si_5	Al	OH_3		O
24	Ca	Mg	Mg	Ti	Al_4	Mg_2		Si_6		OH_3		O
25	Ca	Mg	Mg	Ti	Al_6			Si_6		O_3		OH
26	Ca	Mg	Al	Ti	Al_6			Si_5	Al	O_3		OH

where d_i is an individual bond length, and d_m is the average bond length in each octahedron.

3. Results and discussion

There were 26 different components involving Ti^{4+} at various sites (Tab. 1) calculated using BVTM (ESM 1). Only the Mg-dominant components were evaluated to keep the number of components reasonable. We did not focus on compositions that can be derived from selected components by monovalent substitutions, as these substitutions have no effect on the model. Li-bearing tourmalines were not studied because they usually do not contain a significant amount of Ti.

The stability of selected components was estimated based on several criteria. Firstly, the models were refined to achieve the Bond Valence Sum (BVS) of the O sites as close to 2 *vu* as possible. This allowed us to discriminate components with poor BVS assignment with a difference of more than 0.15 *vu* from 2 *vu*, good BVS assignment with at 0.10–0.15 *vu* difference, and very good with less than 0.10 *vu*. Secondly, the distortion of polyhedra was used to determine components that are not unlikely from a bond-valence perspective but have unusually large distortion. Finally, long-range structure constraints (after Bosi 2018) were used to compare long-range stability with short-range local structure effects.

3.1. Bond-valence topological models

3.1.1. Ti^{4+} at the *Y* site

Titanium in octahedral coordination is, similarly to Al^{3+}, quite small in size in comparison with elements typically occupying the *Y* site, like Mn^{2+}, Li^{+}, Fe^{2+}, Mg^{2+}, or Fe^{3+} (see Tab. 2); however, according to Henry et al. (2011), Ti^{4+} should be exclusively assigned to the *Y* site. The incorporation of Ti^{4+} leads to the shortening of bond lengths and volume compression of the octahedron.

The incorporation of Ti^{4+} into the tourmaline structure often requires the presence of the oxy-component at the *W* site to compensate for the higher sum of positive charges. We tested several possible arrangements of Ti^{4+} at the *Y* site, ($R^{3+}R^{2+}Ti^{4+}$), ($2R^{2+}Ti^{4+}$), ($2R^{3+}Ti^{4+}$), and ($R^{2+}2Ti^{4+}$), always accompanied by heterovalent substitution at other sites to maintain electroneutrality.

We modelled 14 substitutional mechanisms involving Ti^{4+} at the *Y* site (Tab. 3), including all tourmaline groups (sodic, vacant, and calcic) and oxy- and hydroxy-species (fluor-species were not considered). In general, substitu-

Tab. 2 The comparison of the ionic radii of elements in tetrahedral and octahedral coordination (CO) and their bond lengths with oxygen (BL), typically occupying the *Y* and *T* site (values after Hawthorne and Gagné 2024).

	CO [6]	BL [6]	CO [4]	BL [4]
Mn	0.833	2.199	–	–
Li	0.812	2.178	–	–
Fe^{2+}	0.781	2.147	–	–
Fe^{3+}	0.649	2.015	–	–
Mg	0.723	2.089	–	–
Ti	0.605	1.971	0.455	1.821
Al	0.537	1.903	0.380	1.746
Si	–	–	0.259	1.625

tions involving $^{V}O^{2-}_{2-3}$ (11, 14, 22, 25, and 26) showed a strong tendency to underbond O3 (Tab. 3). Even after refining individual bond valence values, the resulting BVS values ranged between 1.464 and 1.665 *vu,* which is insufficient to maintain structural stability. The BVS of the *Y*-site cations showed significant deviations and imbalances, resulting in strongly distorted YO_6 octahedra. Substitution 11 appears to be possible, despite the presence of $^{V}O^{2-}_{2}$.

The ($R^{3+}R^{2+}Ti^{4+}$) arrangement provided three potential mechanisms for Ti^{4+} incorporation – components 8, 10, and 11 (discussed above). The first two showed efficient redistribution of the increased bond valence at the *Y* site (0.49 *vu*) throughout the decrease in bond valences at the *Z* and *T* sites, while maintaining low, comparable distortion indices to those of dravite and dutrowite (Tabs 3 and 5). The components that appeared to be impossible are 4, 14, and 26. Component 4 produced significant overbonding of O1 (2.276 *vu*) and O2 (2.226 *vu*), although this overbonding had no apparent impact on the distortion of the YO_6 octahedron. Component 14, similar to 26, showed underbonding of O3 and was accompanied by overbonding of O6 (Tab. 4); both arrangements also featured increased (nearly doubled) distortion of the *Y* octahedron. The arrangement 18 may be theoretically possible, even though its probability appears lower than that of arrangements 8 and 10 due to a slightly underbonded O5 (1.919 *vu*). Nevertheless, all other bond-valence sums and distortion indices remain within acceptable limits (difference of < 0.05 *vu* and DI < 0.02, respectively).

The ($2R^{2+}Ti^{4+}$) arrangement seems to be the most feasible mechanism for Ti^{4+} incorporation into the tourmaline structure. All proposed substitutions, excluding those with $^{V}O^{2-}$, were reasonable, with component 16 ($^{X}\square\,^{Y}Ti^{X}Na_{-1}\,^{Y}Al_{-1}$) emerging as the most likely (Tab. 3). This mechanism yields well-balanced BVS values at all oxygen sites (1.95–2.02 *vu*), and deviations in cation BVS do not exceed ± 0.05 *vu* (Tabs 3, 4). The calcula-

Tab. 3 The formal and calculated average bond valence of disordered dravite, dutrowite, and substitutional mechanisms involving Ti^{4+} at the *Y* site.

No.	Substitutional mechanism	O1	O2	O3	O4	O5	O6	O7	O8
1.	$^{Y}\square\,^{Y}Al^{Z}Al^{T}Ti^{Y}Mg_{-2}\,^{Z}Mg_{-1}\,^{T}Si_{-1}$	1.947	1.905	1.962	2.066	2.007	1.949	2.053	2.034
2.	$^{T}Ti\,^{T}Si_{-1}$	1.995	2.012	1.961	2.066	2.007	1.972	1.996	1.974
3.	$^{Y}Mg^{Z}Ti^{T}Al^{Y}Al_{-1}\,^{Z}Mg_{-1}\,^{T}Si_{-1}$	2.085	1.861	2.003	2.013	1.934	1.900	2.067	2.090
4.	$^{Y}Ti^{Z}Mg^{T}Al^{Y}Mg_{-1}\,^{Z}Al_{-1}\,^{T}Si_{-1}$	2.276	2.266	1.996	2.013	1.934	1.985	1.897	1.914
5.	$^{Y}Mg^{Z}Ti^{Y}Al_{-1}\,^{Z}Al_{-1}$	2.085	1.861	1.954	2.066	2.007	1.941	2.051	2.030
6.	$^{Z}Ti^{Z}Mg^{Z}Al_{-2}$	2.089	1.995	1.982	2.066	2.007	1.971	1.994	1.970
7.	$^{Y}Ti^{W}O^{Y}Al_{-1}\,^{W}OH_{-1}$	1.942	1.985	1.946	2.066	2.007	2.030	1.996	1.974
8.	$^{Y}Ti^{Z}Mg^{W}O^{Y}Mg_{-1}\,^{Z}Al_{-1}\,^{W}OH_{-1}$	1.903	2.095	1.989	2.066	2.007	2.055	1.939	1.914
9.	$^{Y}Mg^{Z}Ti^{W}O^{Y}Al_{-1}\,^{Z}Mg_{-1}\,^{W}OH_{-1}$	1.135	1.861	2.003	2.066	2.007	1.973	2.109	2.090
10.	$^{Y}Ti^{T}Al^{W}O^{Y}Mg_{-1}\,^{T}Si_{-1}\,^{W}OH_{-1}$	1.903	2.095	2.037	2.013	1.934	2.015	1.954	1.974
11.	$^{Y}Ti^{Z}Al^{T}Al^{V}O_{2}\,^{Y}Mg_{-1}\,^{Z}Mg_{-1}\,^{T}Si_{-1}\,^{V}OH_{-2}$	2.000	2.095	1.947	2.013	1.934	2.046	2.011	2.034
12.	$^{Z}Ti^{V}O_{2}\,^{Z}Mg_{-1}\,^{V}OH_{-2}$	2.005	1.924	1.947	2.066	2.007	2.032	2.109	2.090
13.	$^{Y}Al_{2}\,^{Z}Ti\,^{T}Al^{V}O_{3}\,^{Y}Mg_{-2}\,^{Z}Mg_{-1}\,^{T}Si_{-1}\,^{V}OH_{-3}$	2.025	2.048	1.796	2.013	1.934	2.078	2.067	2.090
14.	$^{Y}Ti^{Z}Al^{V}O_{3}\,^{Y}Mg_{-1}\,^{Z}Mg_{-1}\,^{V}OH_{-3}$	2.006	2.026	1.642	2.066	2.007	2.121	2.053	2.034
15.	$^{Y}Al^{Z}Ti^{V}O_{3}\,^{Y}Mg_{-1}\,^{Z}Mg_{-1}\,^{V}OH_{-3}$	2.010	2.056	1.428	2.066	2.007	2.091	2.109	2.090
16.	$^{X}\square\,^{Y}Ti^{X}Na_{-1}\,^{Y}Al_{-1}$	2.012	2.001	2.056	1.997	1.949	2.015	1.996	1.974
17.	$^{X}\square\,^{Y}Mg^{Z}Ti^{X}Na_{-1}\,^{Y}Al_{-1}\,^{Z}Mg_{-1}$	2.085	2.285	2.003	1.997	1.949	1.958	2.109	2.090
18.	$^{X}\square\,^{Y}Ti^{W}O^{X}Na_{-1}\,^{Y}Mg_{-1}\,^{W}OH_{-1}$	1.993	1.947	2.037	1.997	1.919	2.087	1.996	1.974
19.	$^{X}\square\,^{Y}Ti^{Y}Al^{Z}Al^{T}Al_{2}\,^{W}O\,^{X}Na_{-1}\,^{Y}Mg_{-2}\,^{Z}Mg_{-1}\,^{T}Si_{-2}\,^{W}OH_{-1}$	2.173	2.009	2.133	1.891	1.773	2.033	1.970	2.034
20.	$^{X}\square\,^{Y}Al^{Z}Ti^{T}Al^{W}O^{X}Na_{-1}\,^{Y}Mg_{-1}\,^{Z}Mg_{-1}\,^{T}Si_{-1}\,^{W}OH_{-1}$	1.675	1.838	2.098	1.944	1.846	2.019	2.067	2.090
21.	$^{X}\square\,^{Y}Mg^{Z}Ti_{2}\,^{W}O^{X}Na_{-1}\,^{Y}Al_{-1}\,^{Z}Al_{-1}\,^{Z}Mg_{-1}\,^{W}OH_{-1}$	1.135	1.714	2.058	1.997	1.919	2.000	2.164	2.145
22.	$^{X}\square\,^{Y}Ti_{2}\,^{Z}Al^{V}O_{3}\,^{X}Na_{-1}\,^{Y}Al_{-1}\,^{Y}Mg_{-1}\,^{Z}Mg_{-1}\,^{V}OH_{-3}$	1.972	2.075	1.648	1.997	2.000	2.133	2.053	2.034
23.	$^{X}Ca^{Y}Ti^{T}Al^{W}O^{X}Na_{-1}\,^{Y}Al_{-1}\,^{T}Si_{-1}\,^{W}OH_{-1}$	2.063	2.010	1.990	2.041	2.001	1.955	1.954	1.974
24.	$^{X}Ca^{Y}Ti^{Z}Mg^{W}O^{X}Na_{-1}\,^{Y}Al_{-1}\,^{Z}Al_{-1}\,^{W}OH_{-1}$	2.063	2.010	1.942	2.094	2.075	1.996	1.939	1.924
25.	$^{X}Ca^{Y}Ti^{Z}Al^{V}O_{3}\,^{X}Na_{-1}\,^{Y}Al_{-1}\,^{Z}Mg_{-1}\,^{V}OH_{-3}$	2.021	2.059	1.464	2.094	2.075	2.062	2.053	2.034
26.	$^{X}Ca^{Y}Ti^{Z}Al^{T}Al^{V}O_{3}\,^{X}Na_{-1}\,^{Y}Mg_{-1}\,^{Z}Mg_{-1}\,^{T}Si_{-1}\,^{V}OH_{-3}$	2.006	2.077	1.665	2.041	2.001	2.049	2.011	2.034

Tab. 4 Substitutional mechanisms and calculated bond valence sums at the O1-O8 sites. Green indicates likely components, orange reasonable, and red unlikely.

Arrangement	No.	Substitutional mechanism related to disordered dravite	Y_{formal} (*vu*)	Z_{formal} (*vu*)	T_{formal} (*vu*)	$Y_{calc.}$ (*vu*)	$Z_{calc.}$ (*vu*)	$T_{calc.}$ (*vu*)
Dravite	**0.**	**$Na(Mg_2Al)(Al_5Mg)Si_6O_{18}(BO_3)_3(OH)_3OH$**	**0.39**	**0.47**	**1.00**	**0.38**	**0.48**	**1.01**
Dutrowite	**0.**	**$Na(Fe_{2.5}Ti_{0.5})Al_6Si_6O_{18}(BO_3)_3(OH)_3O$**	**0.39**	**0.50**	**1.00**	**0.42**	**0.47**	**0.99**
$R^{3+}R^{2+}Ti$	4.	$^{Y}Ti^{Z}Mg^{T}Al^{Y}Mg_{-1}{}^{Z}Al_{-1}{}^{T}Si_{-1}$	0.49	0.45	0.96	0.49	0.45	0.97
	8.	$^{Y}Ti^{Z}Mg^{W}O^{Y}Mg_{-1}{}^{Z}Al_{-1}{}^{W}OH_{-1}$		0.45	1.00	0.50	0.45	1.01
	10.	$^{Y}Ti^{T}Al^{W}O^{Y}Mg_{-1}{}^{T}Si_{-1}{}^{W}OH_{-1}$		0.47	0.96	0.50	0.48	0.97
	11.	$^{Y}Ti^{Z}Al^{T}Al^{IV}O_2{}^{Y}Mg_{-1}{}^{Z}Mg_{-1}{}^{T}Si_{-1}{}^{IV}OH_{-2}$		0.50	0.96	0.53	0.51	0.97
	14.	$^{Y}Ti^{Z}Al^{IV}O_3{}^{Y}Mg_{-1}{}^{Z}Mg_{-1}{}^{IV}OH_{-3}$		0.50	1.00	0.51	0.51	1.01
	18.	$^{X}\square{}^{Y}Ti^{W}O^{X}Na_{-1}{}^{Y}Mg_{-1}{}^{W}OH_{-1}$		0.47	1.00	0.50	0.48	1.01
	26.	$^{X}Ca^{Y}Ti^{Z}Al^{T}Al^{IV}O_3{}^{X}Na_{-1}{}^{Y}Mg_{-1}{}^{Z}Mg_{-1}{}^{T}Si_{-1}{}^{IV}OH_{-3}$		0.50	0.96	0.50	0.51	0.96
$2R^{2+}Ti$	7.	$^{Y}Ti^{W}O^{Y}Al_{-1}{}^{W}OH_{-1}$	0.44	0.47	1.00	0.45	0.48	1.01
	16.	$^{X}\square{}^{Y}Ti^{X}Na_{-1}{}^{Y}Al_{-1}$		0.47	1.00	0.44	0.48	1.01
	23.	$^{X}Ca^{Y}Ti^{T}Al^{W}O^{X}Na_{-1}{}^{Y}Al_{-1}{}^{T}Si_{-1}{}^{W}OH_{-1}$		0.47	0.96	0.44	0.48	0.96
	24.	$^{X}Ca^{Y}Ti^{Z}Mg^{W}O^{X}Na_{-1}{}^{Y}Al_{-1}{}^{Z}Al_{-1}{}^{W}OH_{-1}$		0.45	1.00	0.44	0.45	1.01
	25.	$^{X}Ca^{Y}Ti^{Z}Al^{IV}O_3{}^{X}Na_{-1}{}^{Y}Al_{-1}{}^{Z}Mg_{-1}{}^{IV}OH_{-3}$		0.50	1.00	0.44	0.51	1.01
$2R^{3+}Ti$	19.	$^{X}\square{}^{Y}Ti^{Y}Al^{Z}Al^{T}Al_2{}^{W}O^{X}Na_{-1}{}^{Y}Mg_{-2}{}^{Z}Mg_{-1}{}^{T}Si_{-2}{}^{W}OH_{-1}$	0.55	0.50	0.92	0.55	0.51	0.92
$R^{2+}2Ti$	22.	$^{X}\square{}^{Y}Ti_2{}^{Z}Al^{IV}O_3{}^{X}Na_{-1}{}^{Y}Al_{-1}{}^{Y}Mg_{-1}{}^{Z}Mg_{-1}{}^{IV}OH_{-3}$	0.54	0.50	1.00	0.56	0.51	1.01

tions showed that the elevated BVS at the *Y* site (2.64 *vu*), relative to the initial dravite model (2.34 *vu*), can be efficiently redistributed within the tourmaline structure without significantly compromising structural stability. Components 7, 23, and 24 (Tab. 3) also appear feasible; however, all exhibit considerably greater distortion of the YO_6 octahedron compared to the initial model (Tab. 5). The octahedral distortion is, in the case of 23 and 24, partially compensated by the reduction of the tetrahedral distortion.

Substitutions involving ($2R^{3+}Ti^{4+}$) and ($R^{2+}2Ti^{4+}$) are not feasible. Both mechanisms are characterised by substantial underbonding of O4 and O5, and O3, respectively, along with overbonding of O1 and O3, and O6, respectively (Tab. 4). Despite these considerable deviations in oxygen BVS, the distortion indices are only minimally affected (Tab. 5).

3.1.2. Ti^{4+} at the *Z* site

The ionic radii of Ti^{4+} and Al cations in octahedral coordination differ moderately (0.605 and 0.537 Å, respectively, see Tab. 2); therefore, only minor octahedral distortion is expected. Moreover, from the basic bond valence point of view, the *Z* site could be more favourable for Ti^{4+}, because it already accepts the bonds with 0.5 *vu*, which is closer to 0.67 *vu* necessary for accepting Ti^{4+} than the *Y* site with the usual 0.33 *vu* for each bond (Bosi and Andreozzi 2012). Consequently, we modelled 10 substitutional mechanisms with $^{Z}Ti^{4+}$, including sodic and

Tab. 5 The calculated distortion indices (DI) of disordered dravite, dutrowite, and substitutional mechanisms involving Ti^{4+} at the *Y* site. Green indicates likely components, orange reasonable, and red unlikely.

Arrangement	No.	Substitutional mechanism related to disordered dravite	DI *Y*	DI *Z*	DI *T*	DI *X*
Dravite	**0.**	**$Na(Mg_2Al)(Al_5Mg)Si_6O_{18}(BO_3)_3(OH)_3OH$**	**0.022**	**0.017**	**0.008**	**0.045**
Dutrowite	**0.**	**$Na(Fe_{2.5}Ti_{0.5})Al_6Si_6O_{18}(BO_3)_3(OH)_3O$**	**0.019**	**0.016**	**0.011**	**0.043**
$R^{3+}R^{2+}Ti$	4.	$^{Y}Ti^{Z}Mg^{T}Al^{Y}Mg_{-1}{}^{Z}Al_{-1}{}^{T}Si_{-1}$	0.022	0.017	0.010	0.045
	8.	$^{Y}Ti^{Z}Mg^{W}O^{Y}Mg_{-1}{}^{Z}Al_{-1}{}^{W}OH_{-1}$	0.025	0.017	0.008	0.045
	10.	$^{Y}Ti^{T}Al^{W}O^{Y}Mg_{-1}{}^{T}Si_{-1}{}^{W}OH_{-1}$	0.025	0.017	0.010	0.045
	11.	$^{Y}Ti^{Z}Al^{T}Al^{IV}O_2{}^{Y}Mg_{-1}{}^{Z}Mg_{-1}{}^{T}Si_{-1}{}^{IV}OH_{-2}$	0.040	0.017	0.010	0.045
	14.	$^{Y}Ti^{Z}Al^{IV}O_3{}^{Y}Mg_{-1}{}^{Z}Mg_{-1}{}^{IV}OH_{-3}$	0.039	0.017	0.008	0.045
	18.	$^{X}\square{}^{Y}Ti^{W}O^{X}Na_{-1}{}^{Y}Mg_{-1}{}^{W}OH_{-1}$	0.026	0.017	0.008	-
	26.	$^{X}Ca^{Y}Ti^{Z}Al^{T}Al^{IV}O_3{}^{X}Na_{-1}{}^{Y}Mg_{-1}{}^{Z}Mg_{-1}{}^{T}Si_{-1}{}^{IV}OH_{-3}$	0.044	0.017	0.012	0.036
$2R^{2+}Ti$	7.	$^{Y}Ti^{W}O^{Y}Al_{-1}{}^{W}OH_{-1}$	0.040	0.017	0.008	0.045
	16.	$^{X}\square{}^{Y}Ti^{X}Na_{-1}{}^{Y}Al_{-1}$	0.019	0.017	0.006	-
	23.	$^{X}Ca^{Y}Ti^{T}Al^{W}O^{X}Na_{-1}{}^{Y}Al_{-1}{}^{T}Si_{-1}{}^{W}OH_{-1}$	0.036	0.017	0.012	0.036
	24.	$^{X}Ca^{Y}Ti^{Z}Mg^{W}O^{X}Na_{-1}{}^{Y}Al_{-1}{}^{Z}Al_{-1}{}^{W}OH_{-1}$	0.036	0.017	0.010	0.036
	25.	$^{X}Ca^{Y}Ti^{Z}Al^{IV}O_3{}^{X}Na_{-1}{}^{Y}Al_{-1}{}^{Z}Mg_{-1}{}^{IV}OH_{-3}$	0.029	0.017	0.010	0.036
$2R^{3+}Ti$	19.	$^{X}\square{}^{Y}Ti^{Y}Al^{Z}Al^{T}Al_2{}^{W}O^{X}Na_{-1}{}^{Y}Mg_{-2}{}^{Z}Mg_{-1}{}^{T}Si_{-2}{}^{W}OH_{-1}$	0.027	0.017	0.012	-
$R^{2+}2Ti$	22.	$^{X}\square{}^{Y}Ti_2{}^{Z}Al^{IV}O_3{}^{X}Na_{-1}{}^{Y}Al_{-1}{}^{Y}Mg_{-1}{}^{Z}Mg_{-1}{}^{IV}OH_{-3}$	0.032	0.017	0.004	-

Tab. 6 The formal and calculated average bond valence of disordered dravite, dutrowite, and substitutional mechanisms involving Ti^{4+} at the *Z* site. Green indicates likely components, red unlikely.

Arrangement	No.	Substitutional mechanism related to disordered dravite	Y_{formal} (*vu*)	Z_{formal} (*vu*)	T_{formal} (*vu*)	$Y_{calc.}$ (*vu*)	$Z_{calc.}$ (*vu*)	$T_{calc.}$ (*vu*)
Dravite	**0.**	**$Na(Mg_2Al)(Al_5Mg)Si_6O_{18}(BO_3)_3(OH)_3OH$**	**0.39**	**0.47**	**1.00**	**0.38**	**0.48**	**1.01**
	3.	$^{Y}Mg^{Z}Ti^{T}Al^{Y}Al_{-1}{}^{Z}Mg_{-1}{}^{T}Si_{-1}$	0.34		0.96	0.33	0.54	0.97
	9.	$^{Y}Mg^{Z}Ti^{W}O^{Y}Al_{-1}{}^{Z}Mg_{-1}{}^{W}OH_{-1}$	0.34		1.00	0.50	0.45	1.01
	12.	$^{Z}Ti^{V}O_2{}^{Z}Mg_{-1}{}^{V}OH_{-2}$	0.39		1.00	0.39	0.54	1.01
Al_5Ti	13.	$^{Y}Al_2{}^{Z}Ti{}^{T}Al^{V}O_3{}^{Y}Mg_{-2}{}^{Z}Mg_{-1}{}^{T}Si_{-1}{}^{V}OH_{-3}$	0.50	0.52	0.96	0.53	0.54	0.97
	15.	$^{Y}Al^{Z}Ti^{V}O_3{}^{Y}Mg_{-1}{}^{Z}Mg_{-1}{}^{V}OH_{-3}$	0.45		1.00	0.45	0.54	1.01
	17.	$^{X}\square\,{}^{Y}Mg^{Z}Ti^{X}Na_{-1}{}^{Y}Al_{-1}{}^{Z}Mg_{-1}$	0.34		1.00	0.33	0.54	1.01
	20.	$^{X}\square\,{}^{Y}Al^{Z}Ti^{T}Al^{W}O^{X}Na_{-1}{}^{Y}Mg_{-1}{}^{Z}Mg_{-1}{}^{T}Si_{-1}{}^{W}OH_{-1}$	0.45		0.96	0.44	0.54	0.97
Al_4Ti_2	21.	$^{X}\square\,{}^{Y}Mg^{Z}Ti_2{}^{W}O^{X}Na_{-1}{}^{Y}Al_{-1}{}^{Z}Al_{-1}{}^{Z}Mg_{-1}{}^{W}OH_{-1}$	0.34	0.55	1.00	0.33	0.56	1.01
Al_4MgTi	5.	$^{Y}Mg^{Z}Ti^{Y}Al_{-1}{}^{Z}Al_{-1}$	0.34	0.50	1.00	0.33	0.51	1.01
Al_3Mg_2Ti	6.	$^{Z}Ti^{Z}Mg^{Z}Al_{-2}$	0.39	0.47	1.00	0.39	0.48	1.01

vacant tourmaline groups, and oxy- and hydroxy-species (fluor-species were not considered).

Substitutions involving occupancy of 2 or 3 apfu O^{2-} at the *V* site (12, 13, and 15) to compensate for the excess positive charge and maintain electroneutrality exhibited similar behaviour to that observed at the *Y* site. These substitutions resulted in a notable decrease in BVS at O3, reaching values as low as 1.428 *vu* (Tab. 3). Likewise, substitutions with all Mg ordered at the *Y* site (components 3, 5, 9, 17, and 21) confirmed the structural instability of such tourmaline configurations, a phenomenon repeatedly documented in previous studies (Grice and Ercit 1993; Hawthorne 1996, 2002; Bosi and Lucchesi 2007; Bosi and Skogby, 2013; Pieczka et al. 2018; Skřápková et al. 2023). As in dravite or schorl, disorder of divalent cations between the *Y* and *Z* sites is essential to achieve a stable short-range structural arrangement. In these cases, the O2 site showed a pronounced decrease in BVS (down to 1.861 *vu* for mechanisms 3, 5, and 9). Conversely, in mechanism 17, O2 was strongly overbonded (2.285 *vu*), likely due to the vacant *X* site.

The only structurally feasible configuration appears to be $^{Z}(Al_3Mg_2Ti^{4+})$, involving the substitution $^{Z}Ti^{Z}Mg^{Z}Al_{-2}$, which represents a straightforward cation-exchange mechanism. Although this component cannot be regarded as an end-member composition, it exhibits well-balanced BVS values across all oxygen sites and cations, along with low distortion indices (Tabs 6 and 7). The substitution $^{Z}Ti^{Z}Mg^{Z}Al_{-2}$ would result in significant stretching of the *Z*-O bonds due to large cations occupying half of the *Z* sites. This expansion of the local structure can be favourable for the ^{Z}Ti substitution (Bosi and Andreozzi 2012). However, the lower total Al content in this component might limit its occurrence in the natural samples.

3.1.3. Ti^{4+} at the *T* site

Titanium has the same valence as Si; therefore, the BVS at the *T* site remains unchanged. It is important to note, that the probability of Ti^{4+} occupancy at the *T* site is low, as Ti^{4+} strongly prefers incorporation into larger, higher-coordination sites within the tourmaline structure. However, both proposed configurations (1 and 2) appear to be generally feasible; all BVS values fall within acceptable limits, and the distortion indices are negligible (Tabs 8 and 9).

Evidence for the natural occurrence of Ti^{4+} at the *T* site of tourmaline could be derived from bond length

Tab. 7 The calculated distortion indices (DI) of disordered dravite, dutrowite, and substitutional mechanisms involving Ti^{4+} at the *Z* site. Green indicates likely components, red unlikely.

Arrangement	No.	Substitutional mechanism related to disordered dravite	DI *Y*	DI *Z*	DI *T*	DI *X*
Dravite	**0.**	**$Na(Mg_2Al)(Al_5Mg)Si_6O_{18}(BO_3)_3(OH)_3OH$**	**0.022**	**0.017**	**0.008**	**0.045**
Dutrowite	**0.**	**$Na(Fe_{2.5}Ti_{0.5})Al_6Si_6O_{18}(BO_3)_3(OH)_3O$**	**0.019**	**0.016**	**0.011**	**0.043**
	3.	$^{Y}Mg^{Z}Ti^{T}Al^{Y}Al_{-1}{}^{Z}Mg_{-1}{}^{T}Si_{-1}$	0.022	0.016	0.010	0.045
	9.	$^{Y}Mg^{Z}Ti^{W}O^{Y}Al_{-1}{}^{Z}Mg_{-1}{}^{W}OH_{-1}$	0.022	0.016	0.008	0.045
	12.	$^{Z}Ti^{V}O_2{}^{Z}Mg_{-1}{}^{V}OH_{-2}$	0.022	0.014	0.008	0.045
Al_5Ti	13.	$^{Y}Al_2{}^{Z}Ti{}^{T}Al^{V}O_3{}^{Y}Mg_{-2}{}^{Z}Mg_{-1}{}^{T}Si_{-1}{}^{V}OH_{-3}$	0.042	0.016	0.010	0.045
	15.	$^{Y}Al^{Z}Ti^{V}O_3{}^{Y}Mg_{-1}{}^{Z}Mg_{-1}{}^{V}OH_{-3}$	0.016	0.016	0.008	0.045
	17.	$^{X}\square\,{}^{Y}Mg^{Z}Ti^{X}Na_{-1}{}^{Y}Al_{-1}{}^{Z}Mg_{-1}$	0.022	0.016	0.006	–
	20.	$^{X}\square\,{}^{Y}Al^{Z}Ti^{T}Al^{W}O^{X}Na_{-1}{}^{Y}Mg_{-1}{}^{Z}Mg_{-1}{}^{T}Si_{-1}{}^{W}OH_{-1}$	0.027	0.016	0.010	–
Al_4Ti_2	21.	$^{X}\square\,{}^{Y}Mg^{Z}Ti_2{}^{W}O^{X}Na_{-1}{}^{Y}Al_{-1}{}^{Z}Al_{-1}{}^{Z}Mg_{-1}{}^{W}OH_{-1}$	0.022	0.015	0.008	–
Al_4MgTi	5.	$^{Y}Mg^{Z}Ti^{Y}Al_{-1}{}^{Z}Al_{-1}$	0.022	0.016	0.008	0.045
Al_3Mg_2Ti	6.	$^{Z}Ti^{Z}Mg^{Z}Al_{-2}$	0.022	0.016	0.008	0.045

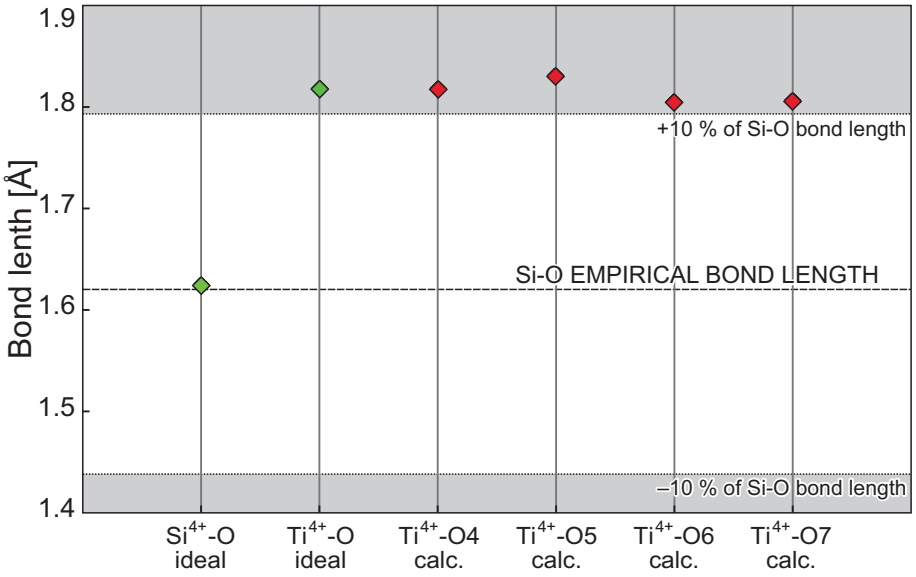


Fig. 3 Calculated bond lengths for ideal Si^{4+}-O, Ti^{4+}-O bonds in the tetrahedral *T*-site coordination of cations and individual modelled Ti^{4+}-O bonds in components 1 and 2. The horizontal dashed line is for the empirical average bond length at the *T* site. The horizontal dotted line is the 10% deviation from the empirical bond length. The "Goldilocks zone" is white. The substitution is significantly limited for cations in the grey zone.

considerations. The substantially larger ionic radius of Ti^{4+} (0.455 Å), nearly twice that of Si (0.259 Å), results in an increase in *T*-O bond lengths. Based strictly on the bond valence, which is not changed by homovalent substitution, it is not expected to induce any significant tetrahedral distortion, although the relaxation of local strain due to the increased *T*-O bond lengths in the neighbouring sites might result in some distortion. This, however, is impossible to calculate based on current knowledge, given the lack of structural data on tourmaline with tetrahedral Ti^{4+}. Consequently, we used the distortion of the Si^{4+}-bearing tetrahedron as a basis for assessing the $Ti^{4+}O_4$ tetrahedron, taking the local neighbourhood into account during model refinement. Our models revealed that the calculated bond lengths are slightly larger than the theoretical tetrahedral Ti-O bond, shifting them outside the "Goldilocks zone" of the *T* site in tourmaline (Fig. 3; Bačík and Fridrichová 2021). This is likely the reason for the Ti^{4+} preference for octahedral sites in tourmaline.

3.2. Bond-valence topological fields

Changes in bond valences and bond lengths induced by Ti^{4+} substitution at various sites can be visualised and studied using the Bond Valence Topological Field method (Bačík 2026). The Bond Valence Topological Field (BVTF) and Bond Length Topological Field (BLTF) were constructed for a structural fragment that included 3 *Y* sites and adjacent 6 *Z* and one *X* site (Figs 2, 4–7, ESM 2). Although there are possible substitutions of Ti^{4+} at the *T* site, these are homovalent and manifest only a difference in the bond lengths in the tetrahedra. The BVTF and BLTF for stable components based on BVS were constructed. The differences between components are more clearly evident in the gradient topological field diagrams (Figs 4–7).

The BVTF and BLTF of disordered dravite are used as a starting point, and all other fields are compared to it (Figs 4–7). Component 1 has a vacancy at the *Y* site, resulting in a significant decrease in both BV and BL.

Tab. 8 The formal and calculated average bond valence of disordered dravite, dutrowite, and substitutional mechanisms involving Ti^{4+} at the *T* site. Green indicates likely component, orange indicates reasonable.

Arrangement	No.	Substitutional mechanism related to disordered dravite	Y_{formal} (*vu*)	Z_{formal} (*vu*)	T_{formal} (*vu*)	$Y_{calc.}$ (*vu*)	$Z_{calc.}$ (*vu*)	$T_{calc.}$ (*vu*)
Dravite	**0.**	**$Na(Mg_2Al)(Al_5Mg)Si_6O_{18}(BO_3)_3(OH)_3OH$**	**0.39**	**0.47**	**1.00**	**0.38**	**0.48**	**1.01**
Si_5Ti	1.	$^{Y}\square\,^{Y}Al^{Z}Al^{T}Ti^{Y}Mg_{-2}{}^{Z}Mg_{-1}{}^{T}Si_{-1}$	0.50	0.50	1.00	0.51	0.51	1.01
	2.	$^{T}Ti^{T}Si_{-1}$	0.39	0.47		0.38	0.48	1.01

Tab. 9 The calculated distortion indices (DI) of disordered dravite, dutrowite, and substitutional mechanisms involving Ti^{4+} at the *T* site. Green indicates likely components, orange indicates reasonable.

Arrangement	No.	Substitutional mechanism related to disordered dravite	DI *Y*	DI *Z*	DI *T*	DI *X*
Dravite	**0.**	**$Na(Mg_2Al)(Al_5Mg)Si_6O_{18}(BO_3)_3(OH)_3OH$**	**0.022**	**0.017**	**0.008**	**0.045**
Dutrowite	**0.**	**$Na(Fe_{2.5}Ti_{0.5})Al_6Si_6O_{18}(BO_3)_3(OH)_3O$**	**0.019**	**0.016**	**0.011**	**0.043**
Si_5Ti	1.	$^{Y}\square\,^{Y}Al^{Z}Al^{T}Ti^{Y}Mg_{-2}{}^{Z}Mg_{-1}{}^{T}Si_{-1}$	0.019	0.017	0.008	0.045
	2.	$^{T}Ti^{T}Si_{-1}$	0.022	0.017	0.008	0.045

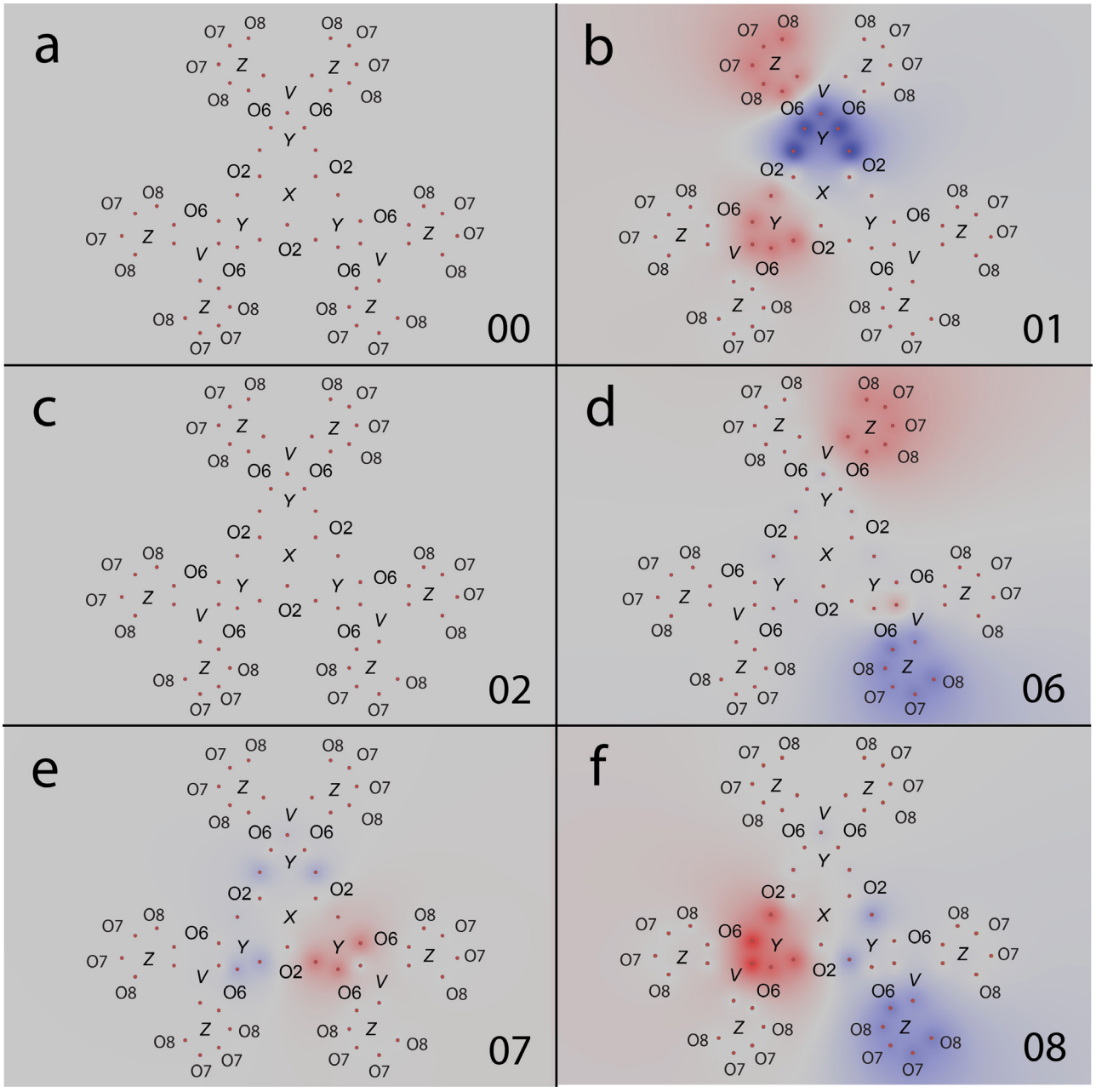


Fig. 4 The gradient bond valence topological fields of components 1–8. Red colour indicates an increase and blue a decrease in bond valence relative to disordered dravite (**a**).

This is compensated for by the substitution of Al for Mg at both the *Y* and *Z* sites, resulting in increased BV and decreased BL (Figs 4b, 5b). The substitution of Ti^{4+} at *T* site does not affect the BVTF and BLTF. Both BVTF and BLTF of component 2 are the same as they are for component 0 because the Ti^{4+} substitution is also at the *T* site and, therefore, does not influence octahedral sites. In the 6 and 8 components, excessive Mg at the *Z* site increases bond lengths and decreases bond valence. However, while no significant compression is observed in 6, Al at the *Y* site compresses the local structure in component 8. Component 7 shows an increase in bond valence resulting from the substitution of Ti^{4+} at the *Y* site. This is compensated by deprotonation at the *W* site, which decreases the neighbouring Mg-O2 bond valences required to balance the Mg BVS. However, due to the increase in bond length due to the $TiAl_{-1}$ substitution, only expansion of the local structure occurs.

In component 10, Ti^{4+} is substituted for ^{Y}Mg, leading to an increase in BV and a decrease in BL at the *Y* site. The substitution requires deprotonation at the *W* site; therefore, there is a slight decrease in BV and an

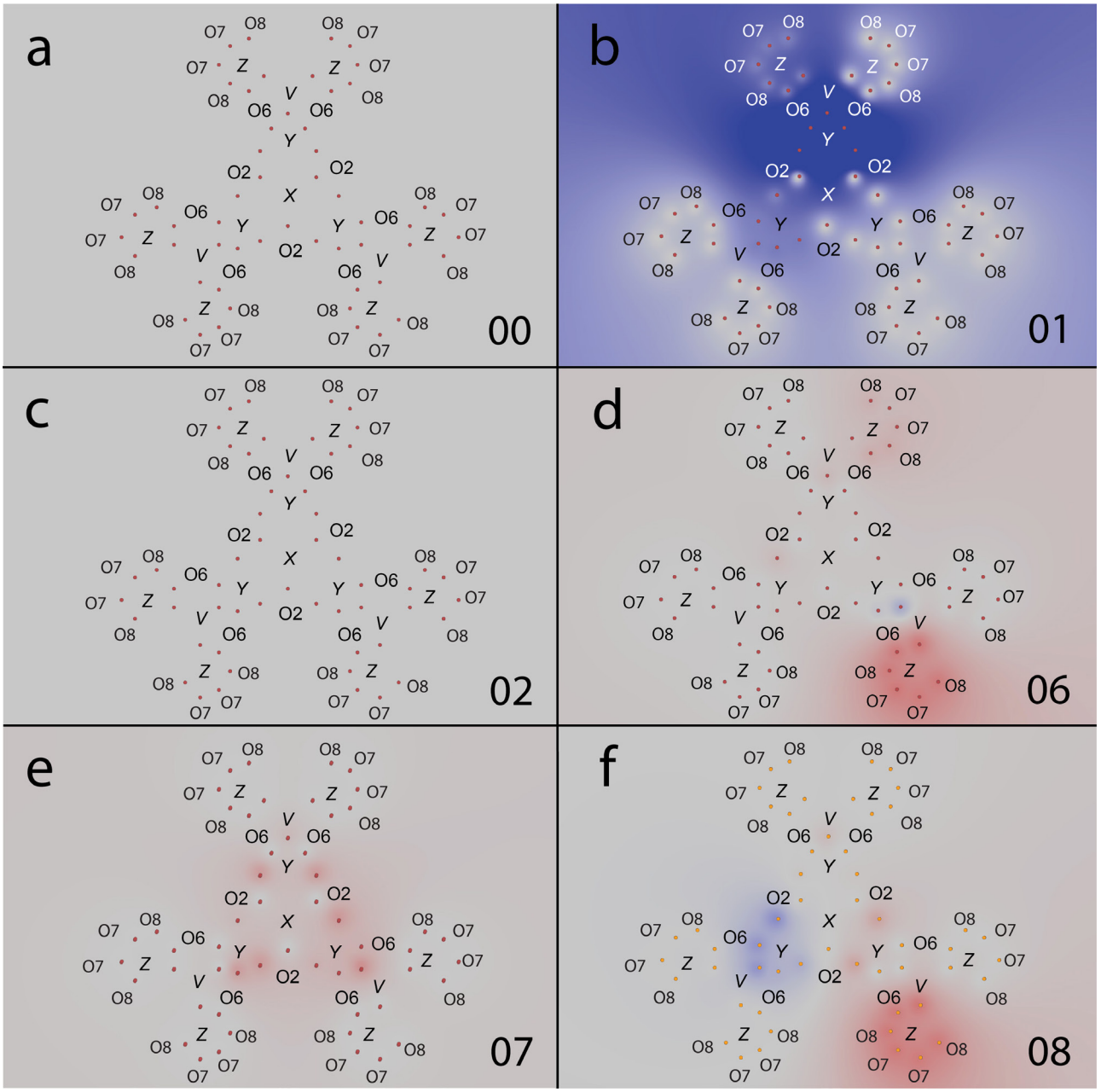


Fig. 5 The gradient bond length topological fields of components 1–8. Red colour indicates an increase and blue a decrease in bond length relative to disordered dravite (**a**).

increase in BL at the neighbouring *Y* sites with Al and Mg. Component 11 is derived from 0 by substitutions at *Y*, *Z*, *T*, and *V* sites. However, to maintain charge balance, only two *V* sites are deprotonated, resulting in a large increase in the BV of the two *Y*-O3 bonds. It was also necessary to increase the BV of the Ti-O2 bond to obtain a BVS for O2 close to 2 *vu*. As a result, the distortion of the *Y* octahedra increased relative to that observed in dravite and dutrowite, and *Y*3 was significantly overbonded (4.36 *vu*), which is not in compliance with a stable structure.

Components 16 and 18 are both *X*-vacant; they differ in *W*-site occupancy and in the substitution of Ti^{4+} at the *Y* site. Component 16 has the substitution of Ti^{4+} for Al, which elevated BV but slightly shortened BL at the *Y* site. In 18, Ti^{4+} substitutes for Mg, resulting in the larger increase in BV and decrease in BL at *Y* (Figs 6c, d, 7c, d).

In contrast, both components 23 and 24 are Ca-bearing. Consequently, *X*-O2 bonds shortened, and their BV increased. This resulted in the opposite behaviour of all *Y*-O2 bonds. The only obvious difference between them

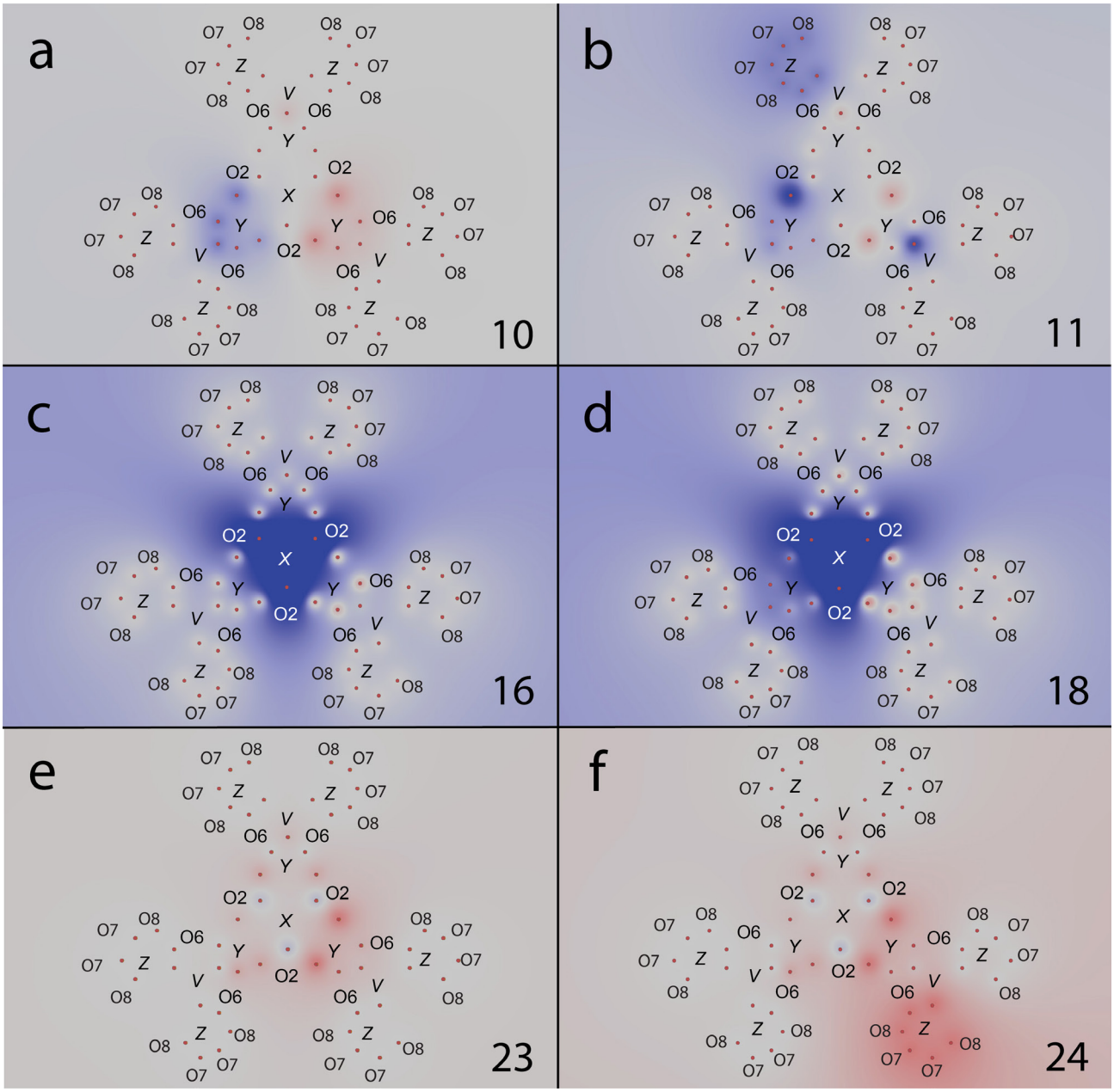


Fig. 6 The gradient bond valence topological fields of components 10–24. Red colour indicates an increase and blue a decrease in bond valence relative to disordered dravite (**a**).

is the additional Mg at the *Z* site in 24, which caused a decrease in BV and prolongation of BL (Figs 6e, f 7e, f).

3.3. Polyhedral distortion

One parameter that is highly useful for assessing structural stability is polyhedral distortion (Robinson et al. 1971; Baur 1974; Wildner 1992; Ertl et al. 2002). This distortion can be caused by structural properties, such as the short- and long-range effects of neighbouring atoms (Bačík 2018; Bosi 2018; Bačík and Fridrichová 2021). The larger the distortion, the less stable the polyhedron.

The distortion of the individual sites has already been discussed; here, we focus specifically on the octahedral distortion and the relations between octahedra based on their distortions. However, it must be noted that distortions calculated from BVTM are purely theoretical. The real structure can relax by additional decrease or increase in the degree of distortion at each polyhedron, which BVTM cannot well predict without actual structural data. Calculated octahedral distortions were compared with the observed values for dutrowite.

However, despite all the above-mentioned shortcomings, the comparison of octahedral distortions is useful

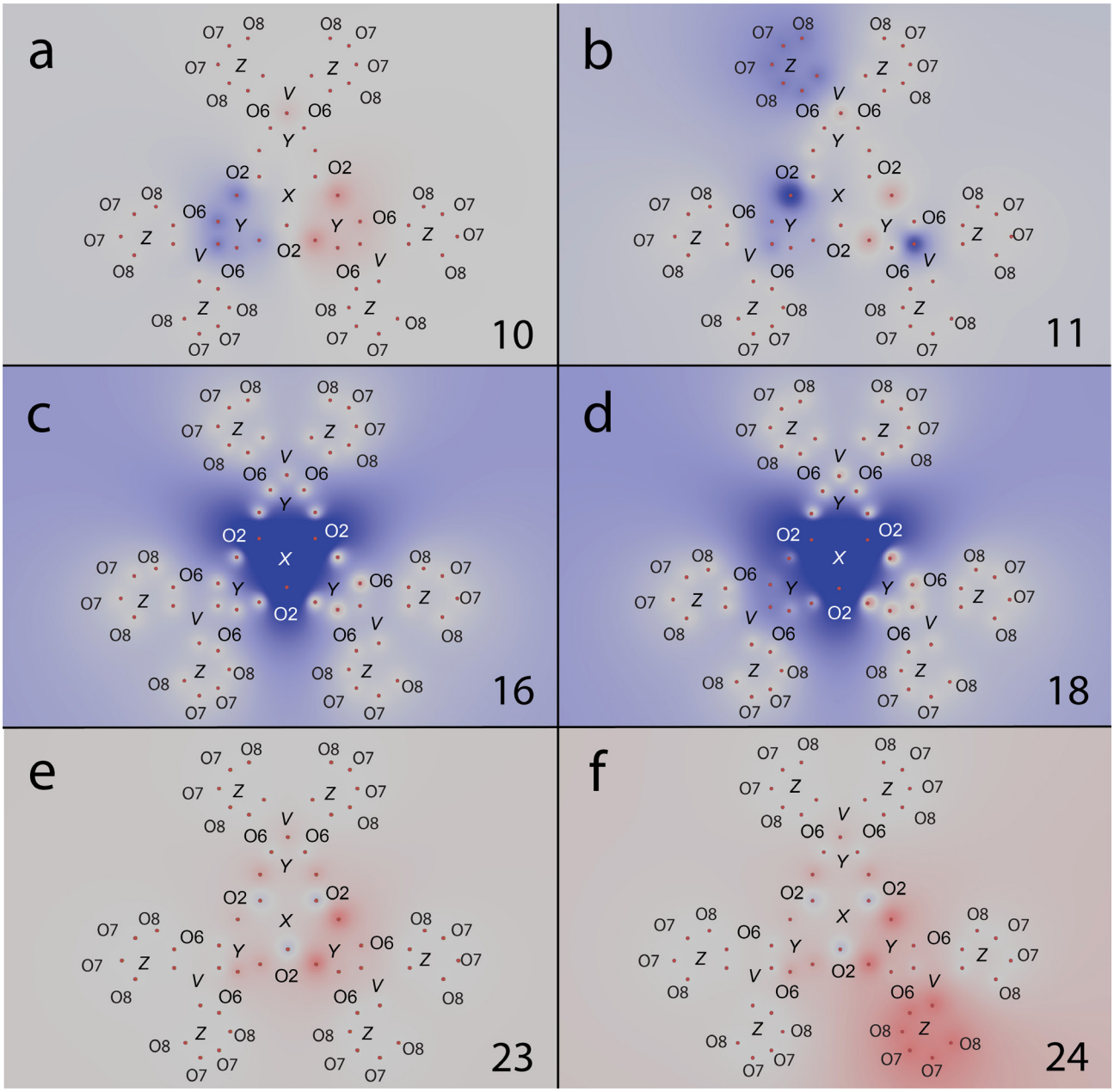


Fig. 7 The gradient bond length topological fields of components 10–24. Red colour indicates an increase and blue a decrease in bond length relative to disordered dravite (**a**)

for distinguishing between stable and potentially unstable geometries (Fig. 8). There was a large variability in DI (*Y*-O) from 0.015 to 0.045, while DI (*Z*-O) varied between 0.014 and 0.017. This is obviously due to the lower variability in *Z*-site occupancy and the fewer distinct arrangements at this site. Only components 12 and 21 show significant deviation, with a very low DI (*Z*-O). Components 12 and 21, as well as other components with lower DI (*Z*-O) (3, 5, 6, 9, 13, 15, 17, and 20), contain Ti^{4+} at the *Z* site. Therefore, it is possible to assume that the presence of Ti^{4+} at the ZO_6 octahedron decreases its distortion. However, no component shows DI (*Z*-O), which would be outside of the range for natural tourmalines of 0.012–0.020 (Ertl et al. 2002).

The YO_6 octahedron of the calculated components has opposite behaviour. Some components exhibit extremely high DI (*Y*-O) values of more than 0.025, the highest observed in natural samples (Ertl et al. 2002). This makes these components very unlikely. It is the case of components 7, 11, 13, 14, 22, 23, 24, 25, and 26. However, all of these except 7, 23, and 24 were already unlikely if the BVS of O1–O8 sites were considered; therefore, it is not surprising in any way that these components have very distorted geometry.

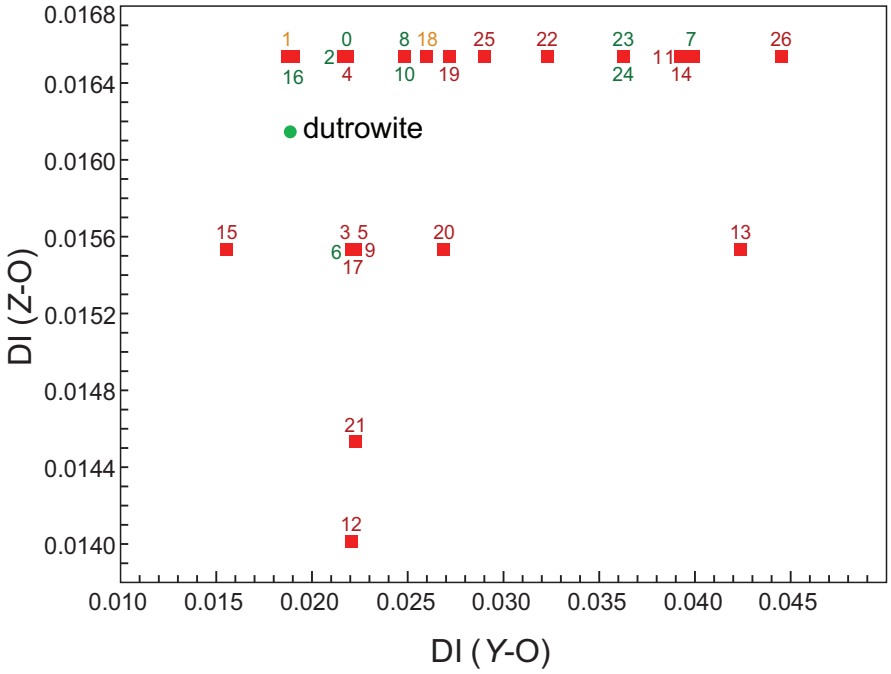


Fig. 8 The comparison of distortion indices at the *Y* and *Z* sites for all modelled components (red squares) and dutrowite (green circle). Green numbers are for components with very good O1–O8 BVS, orange numbers for components with good O1–O8 BVS, and red numbers for components with poor O1–O8 BVS.

Components 7, 22, and 23 have the same $^{Y}(2R^{2+}Ti)$ arrangement and differ only by the occupancy of *X*, *Z,* and *T* sites. We could consider them unlikely, but the real structure could relax their extreme distortion by increasing Al-Mg disorder, resulting in the $^{Y}(R^{3+}R^{2+}Ti)$ arrangement, which has a more optimal DI (*Y*-O) value as evidenced by components 4, 8, and 10. The main reason not to refuse these components, mainly 22 and 23, is the fact that positive correlation of Ti^{4+} and Ca was observed in natural tourmalines on Elba Island, Italy (Dini et al. 2008), in Leinster Granite, Ireland (Gallagher and Kennan 1992), tourmalinites from Velké Žernoseky, Czech Republic (Houzar et al. 2014), the Black Hills, South Dakota, USA (Nabelek 2021), and Zlatá Idka, Slovakia (Bačík et al. 2022), while the components 22 and 23 are likely considering all other factors.

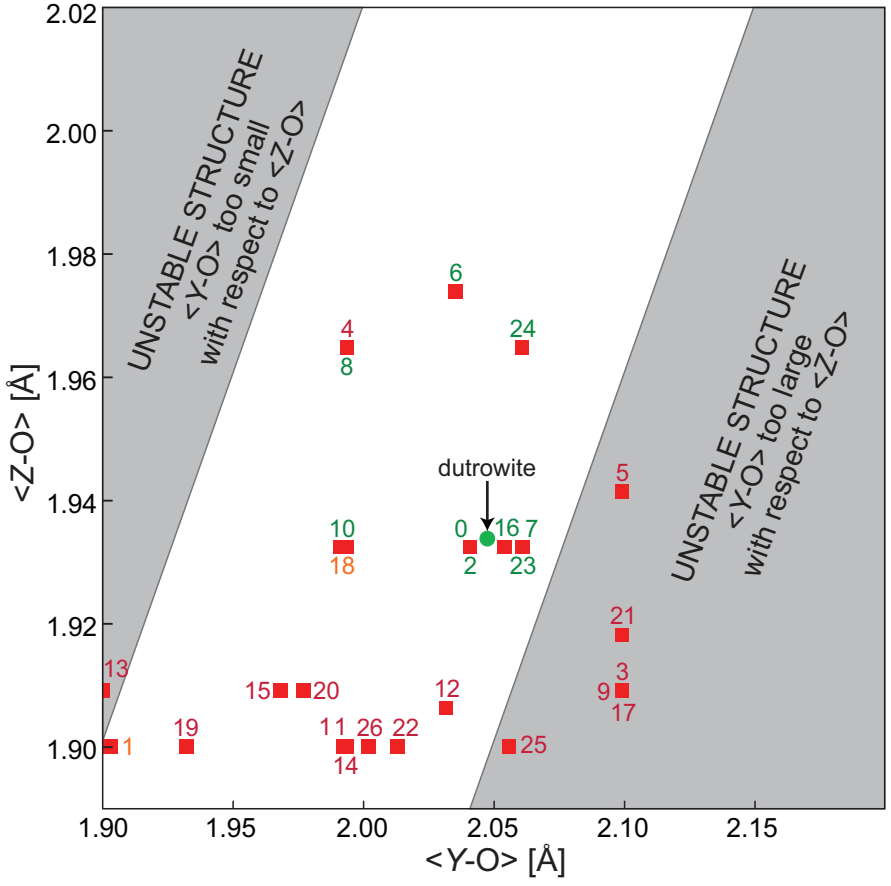


Fig. 9 Comparison of <*Z*-O> and <*Y*-O> defining the possible structural-stability limits of the tourmaline supergroup (after Bosi 2018) with calculated values for all modelled components (red squares) and dutrowite (green circle). Solid diagonal lines are for the ratio 1:1 between <*Z*-O> and <*Y*-O> (left), and the ratio shifted by 0.15 Å (right; after Bosi and Lucchesi 2007). Green numbers are for components with very good O1–O8 BVS, orange numbers for components with good O1–O8 BVS, and red numbers for components with poor O1–O8 BVS.

Tab. 10 Evaluation of the proposed components likelihood based on short-range and long-range constraints.

	Substitutional mechanism	Short-range constraints		Long-range constraints	Likelihood
		O1–O8 BVS	Distortion	<*Y*-O> and <*Z*-O> ratio	
0		Very good	Balanced	Stable	Likely
1	$^{Y}\square^{Y}Al^{Z}Al^{T}\mathbf{Ti}^{Y}Mg_{-2}{}^{Z}Mg_{-1}{}^{T}Si_{-1}$	Good	Balanced	Borderline stable	Reasonable
2	$^{T}\mathbf{Ti}^{T}Si_{-1}$	Very good	Balanced	Stable	Likely
3	$^{Y}Mg^{Z}\mathbf{Ti}^{T}Al^{Y}Al_{-1}{}^{Z}Mg_{-1}{}^{T}Si_{-1}$	Poor	Balanced	Unstable	Unlikely
4	$^{Y}\mathbf{Ti}^{Z}Mg^{T}Al^{Y}Mg_{-1}{}^{Z}Al_{-1}{}^{T}Si_{-1}$	Poor	Balanced	Stable	Unlikely
5	$^{Y}Mg^{Z}\mathbf{Ti}^{Y}Al_{-1}{}^{Z}Al_{-1}$	Poor	Balanced	Unstable	Unlikely
6	$^{Z}\mathbf{Ti}^{Z}Mg^{Z}Al_{-2}$	Very good	Balanced	Stable	Likely
7	$^{Y}\mathbf{Ti}^{W}O^{Y}Al_{-1}{}^{W}OH_{-1}$	Very good	Big DI(*Y*-O)	Stable	Reasonable
8	$^{Y}\mathbf{Ti}^{Z}Mg^{W}O^{Y}Mg_{-1}{}^{Z}Al_{-1}{}^{W}OH_{-1}$	Very good	Balanced	Stable	Likely
9	$^{Y}Mg^{Z}\mathbf{Ti}^{W}O^{Y}Al_{-1}{}^{Z}Mg_{-1}{}^{W}OH_{-1}$	Poor	Balanced	Unstable	Unlikely
10	$^{Y}\mathbf{Ti}^{T}Al^{W}O^{Y}Mg_{-1}{}^{T}Si_{-1}{}^{W}OH_{-1}$	Very good	Balanced	Stable	Likely
11	$^{Y}\mathbf{Ti}^{Z}Al^{T}Al^{V}O_{2}{}^{Y}Mg_{-1}{}^{Z}Mg_{-1}{}^{T}Si_{-1}{}^{V}OH_{-2}$	Very good	Big DI(*Y*-O)	Stable	Reasonable
12	$^{Z}\mathbf{Ti}^{V}O_{2}{}^{Z}Mg_{-1}{}^{V}OH_{-2}$	Poor	Small DI(*Z*-O)	Stable	Unlikely
13	$^{Y}Al_{2}{}^{Z}\mathbf{Ti}^{T}Al^{V}O_{3}{}^{Y}Mg_{-2}{}^{Z}Mg_{-1}{}^{T}Si_{-1}{}^{V}OH_{-3}$	Poor	Big DI(*Y*-O)	Unstable	Unlikely
14	$^{Y}\mathbf{Ti}^{Z}Al^{V}O_{3}{}^{Y}Mg_{-1}{}^{Z}Mg_{-1}{}^{V}OH_{-3}$	Poor	Big DI(*Y*-O)	Stable	Unlikely
15	$^{Y}Al^{Z}\mathbf{Ti}^{V}O_{3}{}^{Y}Mg_{-1}{}^{Z}Mg_{-1}{}^{V}OH_{-3}$	Poor	Balanced	Stable	Unlikely
16	$^{X}\square^{Y}\mathbf{Ti}^{X}Na_{-1}{}^{Y}Al_{-1}$	Very good	Balanced	Stable	Likely
17	$^{X}\square^{Y}Mg^{Z}\mathbf{Ti}^{X}Na_{-1}{}^{Y}Al_{-1}{}^{Z}Mg_{-1}$	Poor	Balanced	Unstable	Unlikely
18	$^{X}\square^{Y}\mathbf{Ti}^{W}O^{X}Na_{-1}{}^{Y}Mg_{-1}{}^{W}OH_{-1}$	Good	Balanced	Stable	Reasonable
19	$^{X}\square^{Y}\mathbf{Ti}^{Y}Al^{Z}Al^{T}Al_{2}{}^{W}O^{X}Na_{-1}{}^{Y}Mg_{-2}{}^{Z}Mg_{-1}{}^{T}Si_{-2}{}^{W}OH_{-1}$	Poor	Balanced	Stable	Unlikely
20	$^{X}\square^{Y}Al^{Z}\mathbf{Ti}^{T}Al^{W}O^{X}Na_{-1}{}^{Y}Mg_{-1}{}^{Z}Mg_{-1}{}^{T}Si_{-1}{}^{W}OH_{-1}$	Poor	Balanced	Stable	Unlikely
21	$^{X}\square\ {}^{Y}Mg^{Z}\mathbf{Ti}_{2}{}^{W}O^{X}Na_{-1}{}^{Y}Al_{-1}{}^{Z}Al_{-1}{}^{Z}Mg_{-1}{}^{W}OH_{-1}$	Poor	Small DI(*Z*-O)	Unstable	Unlikely
22	$^{X}\square^{Y}\mathbf{Ti}_{2}{}^{Z}Al^{V}O_{3}{}^{X}Na_{-1}{}^{Y}Al_{-1}{}^{Y}Mg_{-1}{}^{Z}Mg_{-1}{}^{V}OH_{-3}$	Poor	Big DI(*Y*-O)	Stable	Unlikely
23	$^{X}Ca^{Y}\mathbf{Ti}^{T}Al^{W}O^{X}Na_{-1}{}^{Y}Al_{-1}{}^{T}Si_{-1}{}^{W}OH_{-1}$	Very good	Big DI(*Y*-O)	Stable	Reasonable
24	$^{X}Ca^{Y}\mathbf{Ti}^{Z}Mg^{W}O^{X}Na_{-1}{}^{Y}Al_{-1}{}^{Z}Al_{-1}{}^{W}OH_{-1}$	Very good	Big DI(*Y*-O)	Stable	Reasonable
25	$^{X}Ca^{Y}\mathbf{Ti}^{Z}Al^{V}O_{3}{}^{X}Na_{-1}{}^{Y}Al_{-1}{}^{Z}Mg_{-1}{}^{V}OH_{-3}$	Poor	Big DI(*Y*-O)	Unstable	Unlikely
26	$^{X}Ca^{Y}\mathbf{Ti}^{Z}Al^{T}Al^{V}O_{3}{}^{X}Na_{-1}{}^{Y}Mg_{-1}{}^{Z}Mg_{-1}{}^{T}Si_{-1}{}^{V}OH_{-3}$	Poor	Big DI(*Y*-O)	Stable	Unlikely

3.4. Long-distance structure constraints

Short-range constraints (here bond valences and their sums) control the nearest neighbourhood of atoms at structural sites and thus determine the short-range structure. The stable local arrangements, as building blocks, determine the formation of larger clusters of polyhedra, which can have either ordered or disordered distributions of cations (Bosi 2011). This forms the long-range structure, which is mainly determined by spatial/steric constraints (imposed by translational symmetry) that restrict the number of ion-bonding ways in three-dimensional space. For a long-range structure to be stable, it must satisfy both short-range and long-range constraints. Therefore, all involved short-range arrangements must be consistent with geometrical requirements and with specific long-range interatomic distances (Bosi 2018). This allows for the empirical determination of the long-range stability field based on the structural geometry and size of ions.

In tourmalines, the long-range structural stability can be determined from the ratio of <*Y*-O> and <*Z*-O> bond lengths (Bosi 2018). Their ratio can be expressed by the maximum difference of ca 0.15 Å between <*Y*-O> and <*Z*-O> (Bosi and Lucchesi 2007); the empirical borders are shown in Fig. 9. Based on the empirically determined field of stability, we can refute components 3, 5, 9, 13, 17, 21, and 25 as long-range unstable and unlikely to occur in a tourmaline structure. Component 1 is very near the edge of the stable-structure field, which lowers its likelihood but does not negate it. All other components are likely stable considering long-range constraints. Among them, components 2, 7, 16, and 23 are closest to the natural dutrowite (Biagioni et al. 2023), which increases their likelihood, though it does not make the other components unlikely.

However, comparing the calculated short- and long-range constraints reveals contrasting results. All components with <*Z*-O> below 1.92 Å, including those that seem to be long-range stable, are unstable when short-range constraints are applied. The common feature of these components is *Z*-site occupancy exclusively by Al^{3+}, or by a combination of Al^{3+} and Ti^{4+}. This clearly indicates that in R^{2+}-bearing tourmalines, short-range constraints strictly require a certain (nonzero) degree of R^{2+}-R^{3+} disorder at octahedral sites. A divalent cation, usually Mg^{2+}, stabilizes the local structure. This is clearly different from Li-bearing tourmalines, which can be stable even with $^{Z}Al^{3+}_{6}$ occupancy (Bačík and Ertl 2025).

4. Conclusions

The probability and structural stability of all 26 components were assessed using the BoVaToM 1.2 program, <*Z*-O> vs. <*Y*-O> diagram (Fig. 9), and evaluation of reasonable distortions/bond-length deviations (Figs 3 and 8). On the basis of these criteria, the components were classified into three categories: likely, reasonable, and unlikely (Tab. 10). Most components were designated as having poor calculated bond valences, which were fully consistent with the results of the <*Z*-O> vs. <*Y*-O> diagram. Following this initial selection, only nine components (2, 6, 7, 8, 10, 11, 16, 23, 24) were considered likely, and two (1 and 18) were considered reasonable. Considering the known stability range of distortion parameters, components 7, 11, 23, and 24 were excluded due to the pronounced distortion of their YO_6 octahedra. Subsequently, the diagram illustrating acceptable bond-length deviations at the *T* site (Fig. 3) further reduced the number of the most likely components to six: 2, 6, 8, 10, 16, 18 (plus possibly component 1, which is likely to be only of marginal stability).

The results indicate that the most probable mechanism of Ti^{4+} incorporation into the tourmaline structure involves substitutions at the octahedral sites. The increased bond valence at the *Y* site is efficiently distributed among the remaining sites, resulting in a reasonable adjustment of both bond-valence sums and bond-length values. Incorporation of Ti^{4+} at the *Z* site appears less favourable, yet reasonable. The only acceptable component (6) does not induce any significant structural changes; the slightly elevated BVS values for O1 and O4 remain within reasonable limits. Calculations further show that Ti^{4+} incorporation at the *T* site is unlikely but not impossible; the minor underbonding of O3 and overbonding of O4 remain structurally tolerable.

The incorporation of Ti^{4+} into the tourmaline structure is indisputably feasible; however, its abundance is likely limited. The attempt to introduce two Ti^{4+} atoms per formula unit resulted in substantial distortion of the O_6 octahedron and severe underbonding of O1 and O2 (Tab. 4). Consequently, the structurally tolerable amount of Ti^{4+} is restricted to approximately one *apfu* and is further dependent on the specific chemical composition.

Acknowledgements. The authors are indebted to Aaron Lussier and an anonymous reviewer for their reviews, improving the quality of this paper, and to Ferdinando Bosi for editorial handling. This work was funded by the EU NextGenerationEU through the Recovery and Resilience Plan for Slovakia under the project No. 09I03-03-V04-00060.

References

Bačík P (2018) The crystal-chemical autopsy of octahedral sites in Na-dominant tourmalines: Octahedral metrics model unconstrained by the Y,Z-site disorder assignment. J Geosci 63: 137–154

Bačík P (2026) The Bond Valence Topological Model I: The bond-valence topological map of tourmaline from Forshammar, Sweden. Am Mineral 111: 874–883 DOI: 10.2138/am-2025-9920

Bačík P, Ertl A (2025) How Li can be incorporated into the structure of Al-rich tourmaline. Mineral Mag 89: 791–803 DOI: 10.1180/mgm.2025.28

Bačík P, Fridrichová J (2021) Cation partitioning among crystallographic sites based on bond-length constraints in tourmaline-supergroup minerals. Am Mineral 106: 851–861

Bačík P, Uher P, Sýkora M, Lipka J (2008) Low-Al tourmalines of the schorl-dravite-povondraite series in redeposited tourmalinites from the Western Carpathians, Slovakia. Canad Mineral 46: 1117–1129

Bačík P, Cempírek J, Uher P, Novák M, Ozdín D, Filip J, Škoda R, Breiter K, Klementová M, Ďuďa R, Groat La (2013) Oxy-schorl, $Na(Fe^{2+}{}_2Al)Al_6Si_6O_{18}(BO_3)_3(OH)_3O$, a new mineral from Zlatá Idka, Slovak Republic and Přibyslavice, Czech Republic. Am Mineral 98: 485–492

Bačík P, Ozdín D, Uher P, Chovan M (2022) Crystal chemistry and evolution of tourmaline in tourmalinites from Zlatá Idka, Slovakia. J Geosci 67: 209–222

Baksheev IA, Chitalin AF, Yapaskurt VO, Vigasina MF, Bryzgalov IA, Ustinov VI (2010) Tourmaline in the Vetka porphyry copper-molybdenum deposit, Chukchi Peninsula, Russia. Moscow Univ Geol Bull 65: 27–38

Baur WH (1974) The geometry of polyhedral distortions. Predictive relationships for the phosphate group. Acta Crystallogr B30: 1195–1215

Biagioni C, Bosi F, Mauro D, Skogby H, Dini A, Zaccarini F (2023) Dutrowite, $Na(Fe^{2+}{}_{2.5}Ti_{0.5})Al_6(Si_6O_{18})(BO_3)_3(OH)_3O$, a new tourmaline with Ti as species-forming element. Eur J Mineral 35: 81–94

Bloodaxe ES, Hughes JM, Dyar MD, Grew ES, Guidotti CV (1999) Linking structure and chemistry in the schorl-dravite series. Am Mineral 84: 922–928

Borisov A (2012) The Ti^{4+}/Ti^{3+} ratio of magmatic melts: Application to the problem of the reduction of lunar basalts. Petrology 20: 429–436

Bosi F (2008) Disordering of Fe^{2+} over octahedral sites of tourmaline. Am Mineral 93: 1647–1653

Bosi F (2011) Stereochemical constraints in tourmaline: from a short-range to a long-range structure. Canad Miner 49: 17–27

Bosi F (2018) Tourmaline crystal chemistry. Am Mineral 103: 298–306

Bosi F, Andreozzi GB (2012) A critical comment on Ertl et al. (2012): "Limitations of Fe^{2+} and Mn^{2+} site occupancy in tourmaline: Evidence from Fe^{2+}- and Mn^{2+}-rich tourmaline". Am Mineral 98: 2183–2192

Bosi F, Lucchesi S (2004) Crystal chemistry of the schorl-dravite series. Eur J Mineral 16: 335–344.

Bosi F, Lucchesi S (2007) Structural constraints on chemical variability in the tourmaline group. Am Mineral 92: 1054–1063

Bosi F, Skogby H (2013) Oxy-dravite, $Na(Al_2Mg)(Al_5Mg)Si_6O_{18}(BO_3)_3(OH)_3O$, a new mineral species. Am Mineral 98: 1442–1448

Bosi F, Andreozzi GB, Federico M, Graziani G, Lucchesi S (2005) Crystal chemistry of the elbaite-schorl series. Am Mineral 90: 1784–1792

Bosi F, Reznitskii L, Skogby H (2012) Oxy-chromium-dravite, $NaCr_3(Cr_4Mg_2)Si_6O_{18}(BO_3)_3(OH)_3O$. Am Mineral 97: 2024–2030

Bosi F, Skogby H, Hålenius U, Reznitskii L (2013) Fe-bearing chromo-alumino-povondraite: characterization and relations. Am Mineral 98: 1557–1564

Bosi F, Skogby H, Hovis GL (2023) Crystal chemistry of povondraite. Mineral Mag 87: 178–185

Brown ID (2016) The Chemical Bond in Inorganic Chemistry: The Bond Valence Model. Oxford University Press, vol 27 https://doi.org/10.1093/acprof:oso/9780198742951.001.0001

Cámara F, Ottolini L, Hawthorne FC (2002) Crystal chemistry of three tourmalines. Am Mineral 87: 1437–1442

Clark CM, Hawthorne FC, Ottolini L (2011) Fluor-dravite from the Crabtree Emerald Mine. Canad Mineral 49: 57–62

Da Fonseca-Zang WA, Zang JW, Hofmeister W (2008) The Ti-influence on the tourmaline color. J Braz Chem Soc 19: 1186–1192

Dini A, Mazzarini F, Musumeci G, Rocchi S (2008) Multiple hydrofracturing by B-rich fluids, Elba Island. Terra Nova 20: 318–326

Donnay GH, Buerger MJ (1950) The determination of the crystal structure of tourmaline. Acta Crystallogr 3: 379–388

Ertl A, Hughes JM, Pertlik F, Foit FF Jr, Wright SE, Brandstätter F, Marler B (2002) Polyhedron distortion in tourmaline. Canad Mineral 40: 153–162

Ertl A, Marschall HR, Giester G, Hendry DJ, Schertl HP, Ntaflos T, Luvizotto GL, Nasdala L, Tillmanns E (2010) Ultrahigh-pressure tourmaline: structure and chemistry. Am Mineral 95: 1–10

Ertl A, Schuster R, Hughes JM, Ludwig T, Meyer HP, Finger F, Dyar MD, Ruschel K, Rossman GR, Klötzli U, Brandstätter F, Lengauer CL, Tillmanns E (2012) Li-bearing tourmalines from Austrian pegmatites. Eur J Mineral 24: 695–715

Gadas P, Novák M, Cempírek J, Filip J, Vašinová Galiová M, Groat LA, Všianský D (2014) Feruvitic tourmaline from Mirošov. Canad Mineral 52: 587–603

Gadas P, Novák M, Vašinová Galiová M, Pezzotta F (2023) Tourmalines from Manjaka pegmatite. J Geosci 68: 185–202

Gagné OC, Hawthorne FC (2015) Bond-valence parameters for ion pairs with oxygen. Acta Crystallogr B 71: 562–578.

Gallagher V, Kennan PS (1992) Tourmaline on margin of Leinster Granite. Irish J Earth Sci 11: 131–150

Grice JD, Ercit TS (1993) Ordering of Fe and Mg in tourmaline. Neu Jb Mineral Abh 165: 245–266

Grice JD, Robinson GW (1989) Feruvite: a new tourmaline. Canad Mineral 27: 199–203

Harlaux M, Kouzmanov K, Gialli S, Laurent O, Rielli A, Dini A, Chauvet A, Menzies A, Kalinaj M, Fontboté L (2020) Tourmaline as tracer of fluid evolution, San Rafael deposit. Econ Geol 115: 1665–1697.Hawthorne FC (1996) Light-element variations in tourmaline. Canad Mineral 34: 123–132

Hawthorne FC (2002) Bond-valence constraints on tourmaline chemistry. Canad Mineral 40: 789–797

Hawthorne FC, Gagné OC (2024) New ion radii for oxides, fluorides, chlorides, nitrides. Acta Crystallogr B80: 326–339

Hawthorne FC, Henry DJ (1999) Classification of tourmaline minerals. Eur J Mineral 11: 201–215

Henry DJ, Dutrow BL (1996) Metamorphic tourmaline. Rev Mineral Geochem 33: 503–557

Henry DJ, Novák M, Hawthorne FC, Ertl A, Dutrow BL, Uher P, Pezzotta F (2011) Nomenclature of the tourmaline-supergroup minerals. Am Mineral 96: 895–913

Houzar S, Cempírek J, Toman J, Hrazdil V, Filip J, Radoň M (2014) Turmalinit z Velkých Žernosek (Oparenské krystalinikum, severní Čechy). Bull mineral-petrolog Odd Nar Muz (Praha) 22: 15–24

Jiang S-Y, Palmer MR, McDonald AM, Slack JF, Leitch CHB (1996) Feruvite from the Sullivan deposit. Canad Mineral 34: 733–740

Kommescher S, Kurzweil F, Fonseca ROC, Rzehak LJA, Hohl SV, Kirchenbaur M, Schuth S, Sprung P, Münker C (2023). Mineralogical controls on the Ti isotope composition of subduction zone magmas. Geochem Geophys Geosyst 24: e2022GC010840

Ma C, Rossman GR (2009) Tistarite, Ti_2O_3, a new refractory mineral from the Allende meteorite. Am Mineral 94: 841–844

Ma C, Cámara F, Bindi L, Toledo V, Griffin W (2023) New Minerals from Inclusions in Corundum Xenocrysts from Mt. Carmel, Israel: Magnéliite, Ziroite, Sassite, Mizraite-(Ce) and Yeite. Materials 16: 7578

Nabelek PI (2021) Formation of metasomatic tourmalinites, Black Hills. Am Mineral 106: 282–289

Oliveira B, Griffin WL, Gain SEM, Saunders M, Shaw J, Toledo V, Afonso JC, O'Reilly SY (2021) Ti^{3+} in corundum traces crystal growth in a highly reduced magma. Sci Rep 11: 2439

Pesquera A, Velasco F (1997) Tourmaline-rich rocks from Cinco Villas massif. Contrib Mineral Petrol 129: 53–74

Pesquera A, Torres-Ruiz J, Gil-Crespo PP, Jiang SY (2005) B-isotopic insights into tourmaline-rich rocks, Martinamor. J Petrol 46: 1013–1044

Pieczka A, Ertl A, Sek MP, Twardak D, Zelek S, Szeleg E, Giester G (2018) Oxy-dravite from Wolowa Góra. Mineral Mag 82: 913–928

Pieczka A, Sęk MP, Stachowitz M, Włodek A, Gołębiowska B, Majka J, Woźniak K (2023) Magnesio-dutrowite, IMA 2023-015. Eur J Mineral 35: 659 DOI: 10.5194/ejm-35-659-2023

Povondra P, Lang M, Pivec E, Ulrych J (1998) Tourmaline from Přibyslavice granite. J Geosci 43: 3–8

Robinson K, Gibbs GV, Ribbe PH (1971) Quadratic elongation: A quantitative measure of distortion in coordination polyhedra. Science 172: 567–570

Scribner ED, Groat LA, Cempírek J (2018) Ti-bearing, Al-deficient tourmalines from O'Grady Batholith. J Geosci 63: 123–135

Selway JB, Černý P, Hawthorne FC (1998) Feruvite from Manitoba pegmatites. Canad Mineral 36: 433–439

Skřápková L, Cempírek J, Belley PM, Groat LA, Škoda R (2023) Oxy-dravite from Nunavut. Mineral Mag 87: 719–730

Vereshchagin OS, Wunder B, Baksheev IA, Wilke FDH, Vlasenko NS, Frank-Kamenetskaya OV (2022) Ti^{4+}- and Sn^{4+}-bearing tourmalines: pressure control and comparison of synthetic and natural counterparts. J Geosci 67 (2): 163–171

Watenphul A, Burgdorf M, Schlüter J, Horn I, Malcherek T, Mihailova B (2016) Raman spectroscopy for crystallochemical analyses of tourmaline. Am Mineral 101: 970–985

Wildner M (1992) On the geometry of Co(II)O_6 polyhedra in inorganic compounds. Z Kristallogr – Cryst Mater 202: 51–70

Žáček V, Frýda J, Petrov A, Hyršl J (2000) Povondraite-(oxy)dravite from Bolivia. J Geosci 45: 1–12